nature photonics

SUPPLEMENTARY INFORMATION

https://doi.org/10.1038/s41566-019-0561-9

In the format provided by the authors and unedited.

Higher-order topological states in photonic kagome crystals with long-range interactions

Mengyao Li[1,2], Dmitry Zhirihin[1,3], Maxim Gorlach[3], Xiang Ni[1,2], Dmitry Filonov[4], Alexey Slobozhanyuk[3], Andrea Alù[1,2,5] and Alexander B. Khanikaev[1,2*]

[1]Department of Electrical Engineering, Grove School of Engineering, City College of New York, New York, NY, USA. [2]Physics Program, Graduate Center of the City University of New York, New York, NY, USA. [3]Department of Nanophotonics and Metamaterials, ITMO University, Saint Petersburg, Russia. [4]Center for Photonics and 2D Materials, Moscow Institute of Physics and Technology, Dolgoprudny, Russia. [5]Photonics Initiative, Advanced Science Research Center, City University of New York, New York, NY, USA. *e-mail: khanikaev@gmail.com

Supplementary Information

Higher-order topological states in photonic Kagome crystals with long range interactions

Mengyao Li[1,2], Dmitry Zhirihin[1,3], Maxim Gorlach[3], Xiang Ni[1,2],Dmitry Filonov[4], Alexey Slobozhanyuk[3], Andrea Alù[1,2,5], Alexander B. Khanikaev[1,2,5]

[1]Department of Electrical Engineering, Grove School of Engineering, City College of New York, NY 10031, USA.
[2]Physics Program, Graduate Center of the City University of New York, New York, NY 10016, USA.
[3]Department of Nanophotonics and Metamaterials, ITMO University, St. Petersburg 197101, Russia.
[4]Center for Photonics and 2D Materials, Moscow Institute of Physics and Technology, Dolgoprudny, 141700 Russia
[5]Photonics Initiative, Advanced Science Research Center, City University of New York, New York, NY 10031, USA.

A. Full symmetry analysis of Wannier bands of Kagome lattice

I. Generalized chiral symmetry

Kagome lattice with full symmetry has reflection symmetries, C_3 rotational symmetry, TR symmetry and generalized chiral symmetry, with the last one introduced in our recent work[1]. We briefly summarize the definition of generalized chiral symmetry and its related properties below,

$$\Gamma_3 H_0 \Gamma_3^{-1} = H_1,$$
$$\Gamma_3 H_1 \Gamma_3^{-1} = H_2,$$
$$H_0 + H_1 + H_2 = 0, \quad \text{(A1)}$$

where H_0 is the original Hamiltonian of Kagome lattice, and Γ_3 is the unitary chiral operator, if H_0 meets the conditions in Eq. (A1), the Γ_3 symmetry is preserved. The eigenvalues of Γ_3 are found to be 1, $e^{i2\pi/3}$, and $e^{-i2\pi/3}$. Based on this definition, we have proven that once Γ_3 symmetry is preserved, the system has the following important properties: (1) if $|\psi\rangle$ is an eigenstate, then $\Gamma_3|\psi\rangle$ and $\Gamma_3^2|\psi\rangle$ are also the eigenstates, and the sum of the respective eigenenergies is equal to zero; (2) if zero energy state exists, it is necessarily triply degenerate and has to localize at only one of the sublattices in the coordinate space.

Note that the condition (Eq. A1) should be understood with respect to the ground frequency (energy) level, which is not necessarily zero. Thus, in the case of photonic or acoustic Kagome lattice with the nearest neighbor coupling the ground frequency is defined as the frequency of an individual resonator (site) of the lattice, and the symmetry (Eq. A1) ensures that, if the states with ground energy exist, then they are necessarily triply degenerate.

Even more interestingly, we find out that the inclusion of NNN far-field interactions doesn't break the generalized chiral symmetry. We have confirmed this conclusion both analytically and numerically, as shown by the energy diagram of a finite Kagome lattice as a function of NNN coupling strength J_2/K in Fig. S1, which indicates that these far-field interactions do not destroy the type I corner states keeping them triply degenerate and pinned to the "zero energy" level (the ground frequency).

The generalized chiral symmetry operator can be written as[1]:

$$\Gamma_3 = \begin{pmatrix} 1 & 0 & 0 \\ 0 & e^{i2\pi/3} & 0 \\ 0 & 0 & e^{-i2\pi/3} \end{pmatrix}; \quad \text{(A2)}$$

We first analyze the effect the NNN coupling. In our Kagome system, the NN coupling Hamiltonian has the form

$$\hat{\mathcal{H}}_0 = \begin{pmatrix} 0 & K + Je^{i(\frac{1}{2}k_x + \frac{\sqrt{3}}{2}k_y)\mathrm{a}_0} & K + Je^{-i(\frac{1}{2}k_x - \frac{\sqrt{3}}{2}k_y)\mathrm{a}_0} \\ K + Je^{-i(\frac{1}{2}k_x + \frac{\sqrt{3}}{2}k_y)\mathrm{a}_0} & 0 & K + Je^{-ik_x\mathrm{a}_0} \\ K + Je^{i(\frac{1}{2}k_x - \frac{\sqrt{3}}{2}k_y)\mathrm{a}_0} & K + Je^{ik_x\mathrm{a}_0} & 0 \end{pmatrix} \quad \text{(A3)}$$

while the NNN correction is

$$\hat{\mathcal{H}}_{\mathrm{NNN}} = J_2 * \begin{pmatrix} 0 & e^{ik_x\mathrm{a}_0} + e^{-i(\frac{1}{2}k_x - \frac{\sqrt{3}}{2}k_y)\mathrm{a}_0} & e^{i(\frac{1}{2}k_x + \frac{\sqrt{3}}{2}k_y)\mathrm{a}_0} + e^{-ik_x\mathrm{a}_0} \\ e^{-ik_x\mathrm{a}_0} + e^{i(\frac{1}{2}k_x - \frac{\sqrt{3}}{2}k_y)\mathrm{a}_0} & 0 & e^{-i(\frac{1}{2}k_x - \frac{\sqrt{3}}{2}k_y)\mathrm{a}_0} + e^{-i(\frac{1}{2}k_x + \frac{\sqrt{3}}{2}k_y)\mathrm{a}_0} \\ e^{-i(\frac{1}{2}k_x + \frac{\sqrt{3}}{2}k_y)\mathrm{a}_0} + e^{ik_x\mathrm{a}_0} & e^{i(\frac{1}{2}k_x - \frac{\sqrt{3}}{2}k_y)\mathrm{a}_0} + e^{i(\frac{1}{2}k_x + \frac{\sqrt{3}}{2}k_y)\mathrm{a}_0} & 0 \end{pmatrix} \quad \text{(A4)}$$

This correction obviously belongs to a broader class of corrections leading to the Hamiltonians without coupling within the same sublattice, which is evidenced by vanishing diagonal terms, and whose most general is

$$\hat{\mathcal{H}}_0^{arbi} = \begin{pmatrix} 0 & a_1 & b_1 \\ a_2 & 0 & c_1 \\ b_2 & c_2 & 0 \end{pmatrix} \quad \text{(A5)}$$

We can then calculate the transformed Hamiltonians $\hat{\mathcal{H}}_1^{arbi}$ and $\hat{\mathcal{H}}_2^{arbi}$ to be of the form

$$\hat{\mathcal{H}}_1^{arbi} = \Gamma_3 \hat{\mathcal{H}}_0^{arbi} \Gamma_3^{-1} = \begin{pmatrix} 0 & e^{-i2\pi/3}a_1 & e^{i2\pi/3}b_1 \\ e^{i2\pi/3}a_2 & 0 & e^{-i2\pi/3}c_1 \\ e^{-i2\pi/3}b_2 & e^{i2\pi/3}c_2 & 0 \end{pmatrix}$$

$$\hat{\mathcal{H}}_2^{arbi} = \Gamma_3 \hat{\mathcal{H}}_1^{arbi} \Gamma_3^{-1} = \begin{pmatrix} 0 & e^{i2\pi/3}a_1 & e^{-i2\pi/3}b_1 \\ e^{-i2\pi/3}a_2 & 0 & e^{i2\pi/3}c_1 \\ e^{i2\pi/3}b_2 & e^{-i2\pi/3}c_2 & 0 \end{pmatrix} \quad \text{(A6)}$$

It can be easily observed that $\hat{\mathcal{H}}_0^{arbi} + \hat{\mathcal{H}}_1^{arbi} + \hat{\mathcal{H}}_2^{arbi} = 0$ despite the disparate off-diagonal coupling terms in the Hamiltonian $\hat{\mathcal{H}}_0^{arbi}$. Thus NNN coupling does not break generalized chiral symmetry.

The next correction, which is responsible to the spectral shift of the corner states (with the triple degeneracy preserved), is the third NN coupling within the same sublattice. It can be shown that such interactions are described by the correction of the form

$$\widehat{\mathcal{H}}_{3\mathrm{NN}} = J_3 * 2 * [\cos(k_x \mathrm{a}_0) + \cos\left(\left(\frac{1}{2}k_x + \frac{\sqrt{3}}{2}k_y\right)\mathrm{a}_0\right) + \cos\left(\left(\frac{1}{2}k_x - \frac{\sqrt{3}}{2}k_y\right)\mathrm{a}_0\right)] * \begin{pmatrix} 1 & 0 & 0 \\ 0 & 1 & 0 \\ 0 & 0 & 1 \end{pmatrix} \quad \text{(A7)}$$

which is proportional to the identity matrix. It is obvious that the only effect of this correction is to shift the "zero energy" (ground frequency/energy) due to self-interaction within the same sublattice. This correction is wave-number dependent in the infinite lattice, but it attains a fixed value in the finite structure with corners. As the result, the corner states only exhibit some marginal spectral shift (due to weakness of 3rd NN interactions attributed to the screening by sites of other sublattices in our system) while retaining triple degeneracy. The exact analytic solution for the NN TB model[1] allows to analytically approximate this spectral shift. Thus, the corner state with the only NN coupling is described by the decreasing amplitude which behaves as $\left(-\frac{K}{J}\right)^n$. Assuming that the modes are strongly localized ($\frac{K}{J} \ll 1$), we can use $\frac{K}{J}$ as the small parameter and we can restrict our consideration only to the sites nearest to the corner, in which case the correction takes the value of $4J_3\frac{K}{J}$ for all three corners. Nonetheless, despite the fact that the corner modes retain their triple degeneracy, the chiral symmetry is broken[4] by such interaction within the same sublattice and the corner modes are no longer localized to one sublattice.

We can conclude that the generalized chiral symmetry is present as long as the resonant frequencies of the individual resonators have the same frequency and is not affected by long-range interactions outside the same sublattice. This situation is similar to the case of SSH model where the only two mechanisms to break it are (i) by introducing a detuning in the sublattice energies ($\epsilon_a \neq \epsilon_b$) described by the $\hat{\sigma}_z$ term of the SSH Hamiltonian or (ii) by even (long-range) interactions within the same sublattice[4]. Interestingly, the first class of perturbations would immediately lift the degeneracies of the edge and corner states in bipartite 1D SSH model or tripartite 2D Kagome lattice, respectively. The second class of perturbations, on the other hand, does not lift this degeneracy. At the same time, long-range interactions, while breaking the chiral symmetry, do not render the topological invariant (bulk polarization) meaningless as it happens for the first class of perturbation with on-site energy detuning[4]. To summarize, the symmetry breaking terms reducing the generalized chiral symmetry, which have the form

$$\hat{O}_1 = \begin{pmatrix} 1 & 0 & 0 \\ 0 & -1 & 0 \\ 0 & 0 & 0 \end{pmatrix}, \hat{O}_2 = \begin{pmatrix} 0 & 0 & 0 \\ 0 & 1 & 0 \\ 0 & 0 & -1 \end{pmatrix}, \hat{O}_3 = \begin{pmatrix} 1 & 0 & 0 \\ 0 & 1 & 0 \\ 0 & 0 & -1 \end{pmatrix}, \hat{O}_4 = \begin{pmatrix} -1 & 0 & 0 \\ 0 & 1 & 0 \\ 0 & 0 & 1 \end{pmatrix} \quad \text{(A8)}$$

are not induced by the long-range interactions and, therefore, the triple degeneracy is preserved.

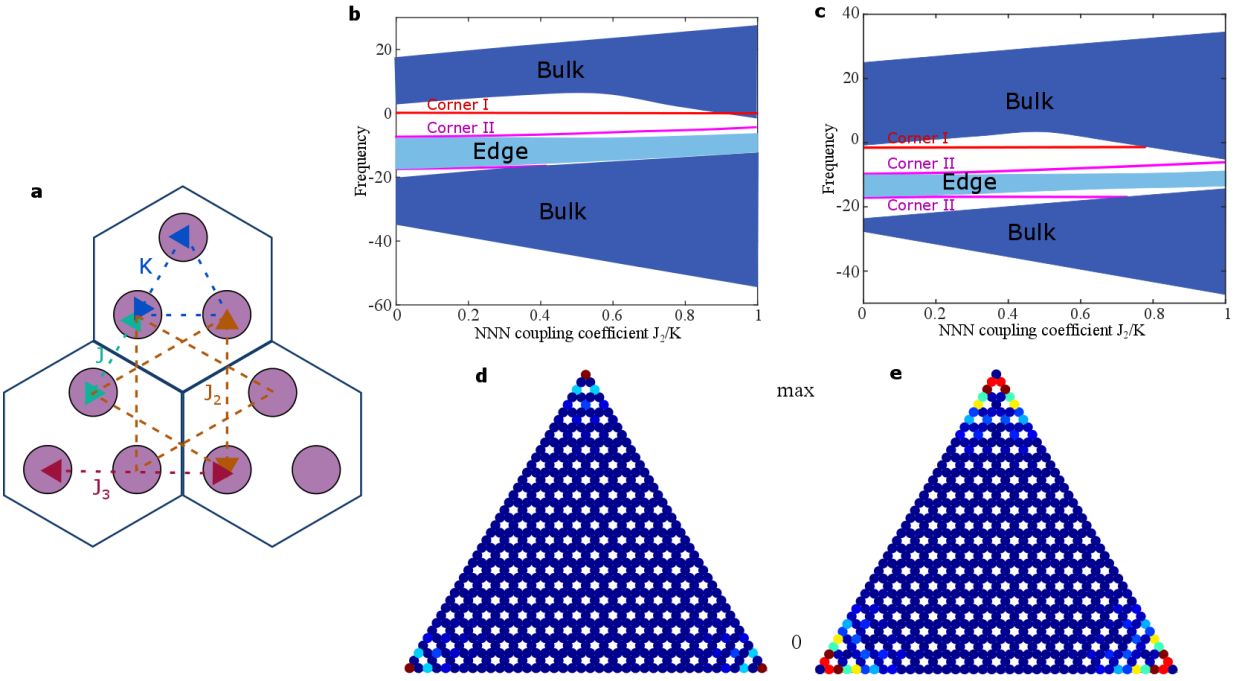

Fig S1| Tight binding calculations with long-range interactions considered. $J/K = 2.5$ in this system. **a** Coupling scheme in Kagome lattice. Intra-cell coupling K, inter-cell coupling J, NNN coupling J_2, and 3rd NN coupling J_3 are marked on the graph. **b** Energy spectrum of finite triangle of Kagome structure with nonzero NNN coupling. **c** Energy spectrum of Kagome finite triangle structure with up to 3rd NN coupling. Constant value of $J_3 = 0.25K$ is applied. **d**, **e** corner states (I and II) field profile in TB calculation up to NNN coupling. We used $J_2/K = 0.6$ in this case making sure the upper bulk band doesn't merge with corner states.

II. Bulk polarization

The relevant quantity to characterize the topology of bands in the Kagome lattice with full symmetry is the bulk polarization, which is defined as[2]

$$p_s = 1/N_k \sum_{j,k_t} v_s^j(k_t), \tag{A9}$$

where $v_s^j(k_t)$ is the eigenvalue (Wannier center) of the Wilson loop, which is defined as $W_{2\pi+k_s \leftarrow k_s, k_t} = \langle u_{2\pi+k_s,k_t} | u_{2\pi+k_s-\delta k,k_t} \rangle \langle u_{2\pi+k_s-\delta k,k_t} | u_{2\pi+k_s-2\delta k,k_t} \rangle \dots \langle u_{k_s+2\delta k,k_t} | u_{k_s+\delta k,k_t} \rangle \langle u_{k_s+\delta k,k_t} | u_{k_s,k_t} \rangle$, and $k_s, k_t = 0, \delta k, \dots, (N_k - 1)\delta k$, $\delta k = \frac{1}{N_k} \frac{4\pi}{\sqrt{3}a}$. j represents the index of the occupied bands, $j = 1,2, \dots, N_o$. Following the above formula, we evaluate the Wannier bands corresponding to the lowest energy band of Kagome lattices with full symmetry, without and with NNN hopping included, which are shown in Fig. S2. In the trivial case, that is, when the inter-cell coupling K is larger than intra-cell coupling J (shrunken lattice), the zero value of bulk polarization indicates modes pinned to the center of every unit cell, and hence there are no modes localized at the boundaries. However, in the topologically nontrivial case (K<J) (expanded lattice), the bulk

polarization is nonzero (1/3 for the Kagome lattice with full symmetries, i.e. C_3 rotational symmetry, TR symmetry and the generalized chiral symmetry being present), giving rise to the modes at the boundaries away from the bulk as well as to localized states (including corner states) at the appropriate sites at the boundaries of the structure. Note the NNN hopping does not destroy bulk polarization, instead, it is still preserved and quantized as 1/3 in the nontrivial case. The same is true for the case of 3rd order coupling with hopping within the same sublattice. While topological polarization can still de defined, this type of perturbations changes the class of the system from BDI to AI, which makes it impossible to establish bulk-edge correspondence[4] and to reliably predict the presence of boundary modes, especially in the regime of the strong symmetry breaking.

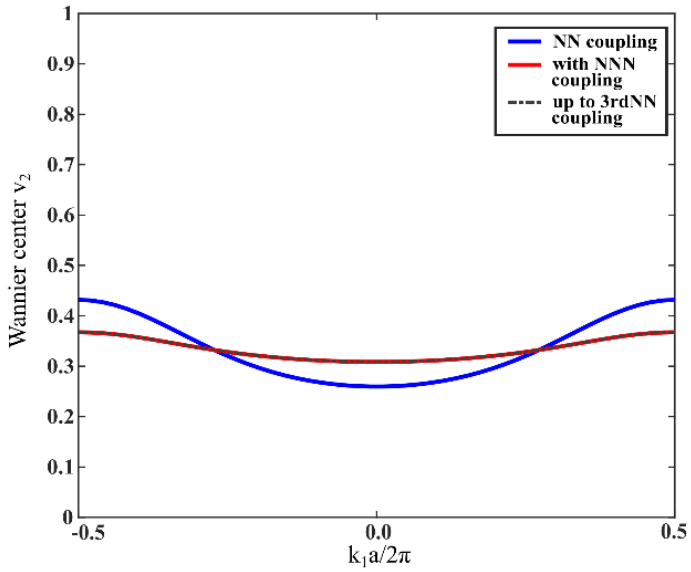

Fig S2| Wannier bands in TBM for the cases of Kagome lattice with only nearest neighbour (NN) coupling considered, with both NN and NNN coupling considered, and considering up to 3rd nearest order coupling in topological expanded Kagome lattice. For both cases, the bulk polarization is quantized as 1/3. $J/K = 2.5$ is used in this calculation, and when NNN coupling is applied, NNN coupling strength versus intra-cell coupling strength is fixed at $J_2/K = 0.6$, and 3rd NN coupling versus NNN coupling is given by $J_3/J_2 = 0.6$.

Symmetry constraints over bulk polarization

In general, the symmetry operator over the Wilson loop satisfies the following relation[3]

$$\boldsymbol{B}_{g,k_j} W_{l_i,k_j} \boldsymbol{B}^{\dagger}_{g,k_j} = W_{D_g l_i, D_g k_j}, \tag{A10}$$

l_i is the starting point of the path in the Brillouin zone, where $\boldsymbol{B}^{n,m}_{g,\boldsymbol{k}} = \langle u^n_{D_g \boldsymbol{k}} | g_{\boldsymbol{k}} | u^m_{\boldsymbol{k}} \rangle$ is the unitary sewing matrix in which the unitary operator $g_{\boldsymbol{k}}$ transforms the Hamiltonian following the formula

$$g_{\boldsymbol{k}} h_{\boldsymbol{k}} g^{\dagger}_{\boldsymbol{k}} = h_{D_g \boldsymbol{k}}, \tag{A11}$$

and the symmetry operator D_g transforms $\boldsymbol{k}$ to $D_g\boldsymbol{k}$.

Based on Eqs. (A10-A11), we performed the analysis of symmetry constraints over bulk polarization[1] for the Kagome lattice with full symmetry, and these constraints are summarized below:

Constraint of reflection symmetries $\mathrm{M_i}$ *over* $\mathrm{v_i(k_j)}$

$$\mathrm{M}_i: v_i(k_j) = v_i(k_t) \text{ mod } 1. \tag{A12}$$

Therefore, under the reflection operation $\mathrm{M_i}$, the bulk polarizations between different paths in Brillouin zone have the relation

$$\mathrm{M}_i: p_{i,l_j} = p_{i,l_t}. \tag{A13}$$

Constraint of reflection symmetries $\mathrm{M_i}$ *over* $\mathrm{v_j(k_t)}$

$$\mathrm{M}_i: v_j(k_t) = v_t(k_j) \text{ mod } 1. \tag{A14}$$

Accordingly, the polarization of the lowest energy band is

$$\mathrm{M}_i: p_j = p_t, \tag{A15}$$

Constraint of C_3 *symmetry over* $v_i(k_j)$

The Wannier bands under C_3 symmetry satisfy the condition

$$C_3: v_i(k_j) = v_j(k_t) \text{ mod } 1. \tag{A16}$$

And due to the equivalence of the three reciprocal lattice vectors of Kagome lattice, the polarizations of the bands for the three choices are equivalent

$$C_3: p_i = p_j = p_t. \tag{A17}$$

Constraint of time reversal symmetry T *over* $v_i(k_j)$.

The time reversal operator flips the sign of momentum vector due to antilinear property of the operator,

$$T: v_i(k_j) = v_i(-k_j). \tag{A18}$$

Therefore, on the polarization

$$T: p_i(k_j) = p_i(-k_j). \tag{A19}$$

If the direction of path integration in momentum space is reversed, $W_{c_i,k_j} \rightarrow W_{-c_i,k_j}$, the Wannier center changes correspondingly

$$v_i(k_j) = -v_{-i}(k_j). \tag{A20}$$

Based on these equations, the polarization of bands for the Kagome lattice is determined solely by the constraints of spatial symmetries and TR symmetry, and the absolute value for the lowest energy band is quantized as

$$|p_i| = \frac{1}{3}, 0. \quad \text{(A21)}$$

As long as the interactions don't break the symmetries analyzed above, the same analysis should apply, and the NNN hopping (just like NN hopping) indeed preserves these symmetries, which implies that the inclusion of NNN interactions (and higher order couplings, as long as they are isotropic) does not affect the quantization of bulk polarization (1/3 or 0). Similarly, the Wannier band does not change compared to the NNN case when 3rd NN coupling is considered.

B. Verification of the existence of the topological states for the open system and the system bounded by a conductor. Numerical and experimental results.

One important distinction between electromagnetic and condensed matter topological system resides in the boundary conditions that may terminate a finite system. The boundary conditions can have detrimental effects on corner or edge states, e.g., they can break the symmetry responsible for the very emergence of topological boundary states, thus destroying these states or rendering them trivial.

Therefore, in addition to the geometry of topological Kagome crystal surrounded by the trivial domain of the main text, we have experimentally investigated the case of open system and the system bounded by a conducting boundary. To this aim we first have removed trivial crystal domain from the lateral sides of the structure. This lead to the out-coupling of modes of the structure to the modes of the parallel-plate waveguide (continuum of the guided modes) – the interaction which may potentially be detrimental for topological boundary states. In the second experiment, we have surrounded the crystal with aluminum walls across the waveguide thickness, in which case the modes remain confined to the topological domain and the leakage into the waveguide is completely suppressed.

With the goal to verify the presence of topological states in these systems we performed the experimental measurements in the microwave frequency range using the same near-field scanning technique as for the case outlined in the main text. The results for the case of open topological crystal are shown in Fig. S3 which displays the measured near-field maps for three types of topological boundary modes: edge, corner type I and corner type II alongside with the results of numerical calculations. The experimental results are found to be in an excellent agreement with the numerical predictions which proves that the emergence of both type of HOT states is independent of the applied boundary conditions. As can be seen, the topological modes still persist in the open systems in spite of leakage into the parallel-plate waveguide, although we do observe spectral broadening of the corner states due to the radiative leakage, which leads to the shorter lifetime of the modes. Thus we conclude that the open character of the system does not destroy the HOT states but only leads to their spectral broadening.

For the case of the topological crystal surrounded by metal boundary the results of numerical and experimental studies are presented in Fig. S4 and Fig. S5, respectively. As can be seen from Fig. S4, the topological modes still persist, although we do observe spectral shift of boundary modes due to their interaction with the metal (Fig. S4**a**). Specifically, the type I corner states exhibit spectral redshift as we move deeper into topological domain by increasing inter- to intra-cell coupling ratio (Fig. S4**a**). This shift clearly indicates that the generalized chiral symmetry is broken, which is also evidenced by some penetration of the field of the mode into adjacent sublattices seen both in theory and experimental results. Thus, we conclude that, while the conducting boundaries do not destroy the corner states, they do break generalized chiral symmetry leading to the spectral shift of the boundary modes.

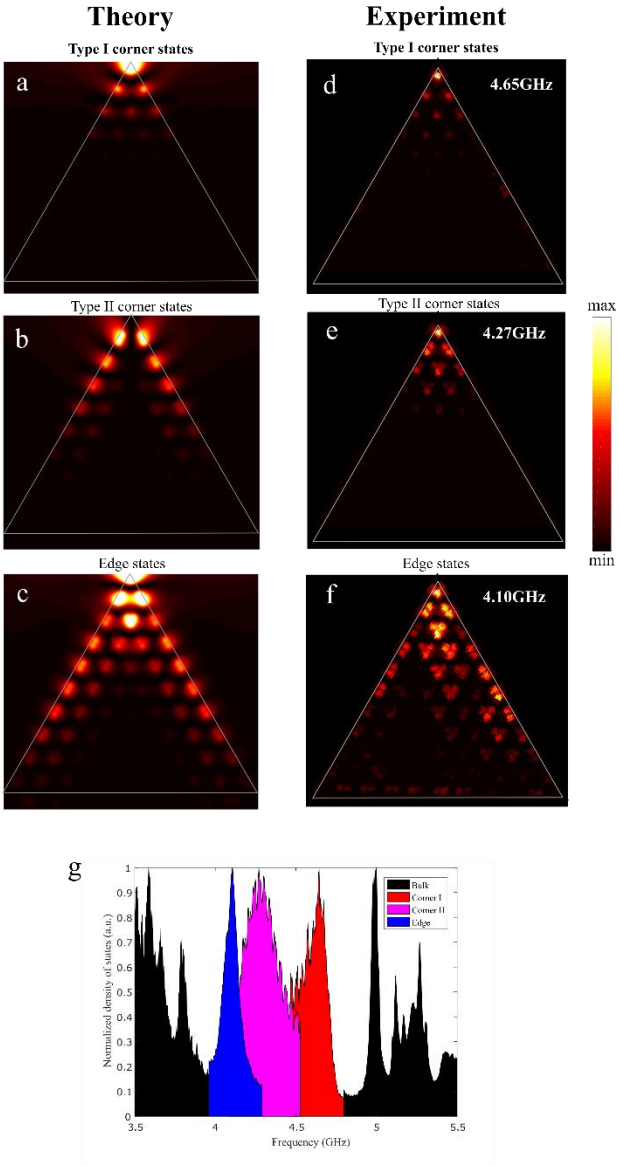

Fig. S3| **Experimental observation of topological states and density of corner, edge and bulk states for open system. a** Retrieved density of states from experimental results. **b**, **c** and **d** represents near-field

profiles of two different types of corner states and edge state. The system is excited by a source placed at the left bottom corner.

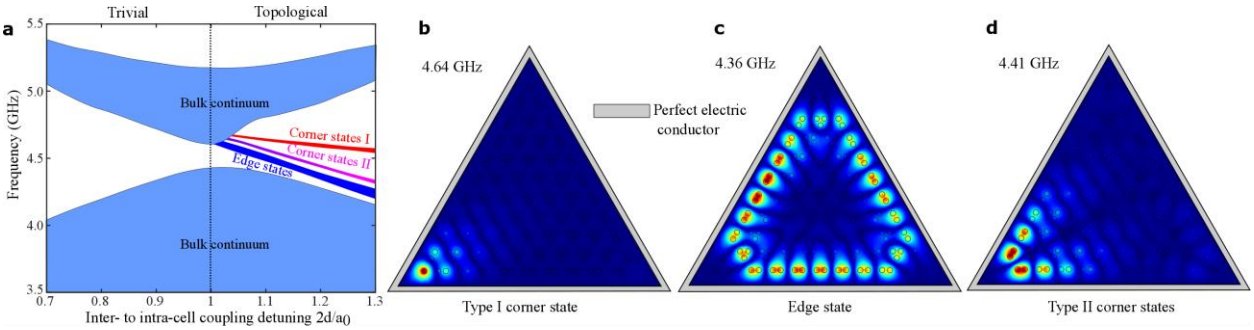

Fig. S4| **Simulation results of topological edge states and type I&II corner states with perfect electric conductor (PEC) boundary condition.** **a** Energy spectrum for triangle Kagome lattice with coupling detuning parameter $\kappa = 2d/a_0$. **b**, **c** and **d** showing the field profiles and their corresponding frequencies. Both corner states (type I as red band and type II as magenta band in **a**) and edge states (dark blue band in **a**) appear in band gap of topological region. Corner states I and II are both triply degenerated states.

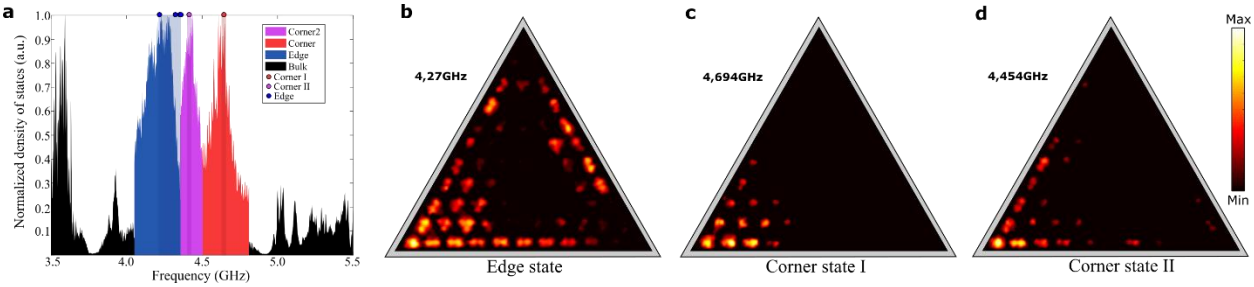

Fig. S5| **Experimental observation of HOT Type I and Type II corner states with metallic boundary.** **a** Density of states experimental results and comparison to eigenstate simulations. Coloured areas are experimental results of corner excitation, and corresponding coloured dots at the top of the figure are first principle calculations of the eigenvalues for the same structure. **b**, **c** and **d** different types of topological corner and edge state observed in experiment at corresponding frequencies when the system is excited by a source placed at the left bottom corner, log scaled field profiles from experiment are shown in these figures.

C. Analytical description of corner states in Kagome lattice mediated by the next-nearest neighbor coupling

I. Problem setting

Since the unit cell of Kagome lattice includes three sites, we can adopt the basis $|\psi\rangle = (a, b, c)^T$ with the amplitudes a, b and c illustrated in Fig. S6 and present Bloch Hamiltonian in the form

$$\hat{H} = \hat{H}_0 + \hat{H}_{NNN}. \quad \text{(C1)}$$

Here $\hat{H}_0$ part is associated with the nearest-neighbor coupling

$$\hat{H}_0 = -\begin{pmatrix} 0 & K + Je^{i(\frac{1}{2}k_x + \frac{\sqrt{3}}{2}k_y)} & K + Je^{-i(\frac{1}{2}k_x - \frac{\sqrt{3}}{2}k_y)} \\ K + Je^{-i(\frac{1}{2}k_x + \frac{\sqrt{3}}{2}k_y)} & 0 & K + Je^{-ik_x} \\ K + Je^{i(\frac{1}{2}k_x - \frac{\sqrt{3}}{2}k_y)} & K + Je^{ik_x} & 0 \end{pmatrix} \quad \text{(C2)}$$

and $\hat{H}_{NNN}$ describes the coupling of the next nearest neighbors:

$$\hat{H}_{NNN} = -J_2 \begin{pmatrix} 0 & e^{ik_x} + e^{-i\left(\frac{1}{2}k_x - \frac{\sqrt{3}}{2}k_y\right)} & e^{i\left(\frac{1}{2}k_x + \frac{\sqrt{3}}{2}k_y\right)} + e^{-ik_x} \\ e^{-ik_x} + e^{i\left(\frac{1}{2}k_x - \frac{\sqrt{3}}{2}k_y\right)} & 0 & e^{-i\left(\frac{1}{2}k_x - \frac{\sqrt{3}}{2}k_y\right)} + e^{-i\left(\frac{1}{2}k_x + \frac{\sqrt{3}}{2}k_y\right)} \\ e^{-i\left(\frac{1}{2}k_x + \frac{\sqrt{3}}{2}k_y\right)} + e^{ik_x} & e^{i\left(\frac{1}{2}k_x - \frac{\sqrt{3}}{2}k_y\right)} + e^{i\left(\frac{1}{2}k_x + \frac{\sqrt{3}}{2}k_y\right)} & 0 \end{pmatrix}, \quad \text{(C3)}$$

where the choice of the coordinate system is depicted in Fig. S6, and the lattice period is equal to 1.

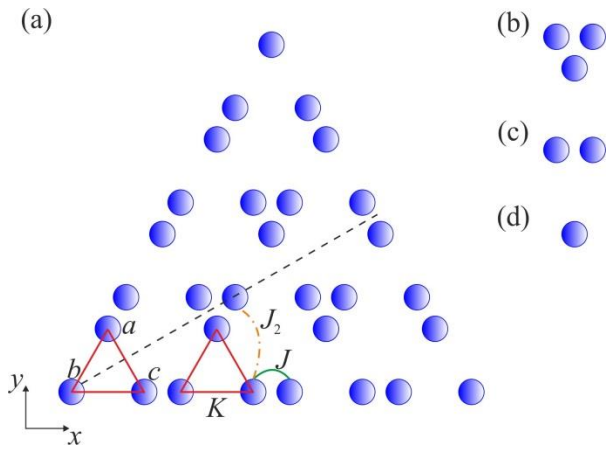

Fig. S6| (a) Illustration of Kagome lattice geometry. Red triangles show the boundaries of the unit cell, black dashed line is the bisectrix of the corner. (b-d) If $K = J_2 = 0$, the lattice splits into isolated set of coupled (b) trimers in the bulk; (c) dimers at the edge; (d) single isolated sites at the corners. In what follows we consider the terms proportional to K and J_2 as a perturbation.

Solving an eigenvalue equation $\hat{H}|\psi\rangle = E|\psi\rangle$, we can immediately obtain the dispersion $E(k_x, k_y)$ of the bulk modes in a two-dimensional lattice. In the case of a finite lattice tight-binding $N \times N$ Hamiltonian is used instead, where N is the total number of sites. Our goal here is to provide a theoretical interpretation of the corner states which emerge in the system Fig. S6 due to the nonzero next-nearest neighbor hopping J_2.

II. Eigenstates of the lattice in the case $K = J_2 = 0$

In the limiting case when $K = J_2 = 0$, an entire lattice splits into isolated clusters of sites connected with each other only via J links.

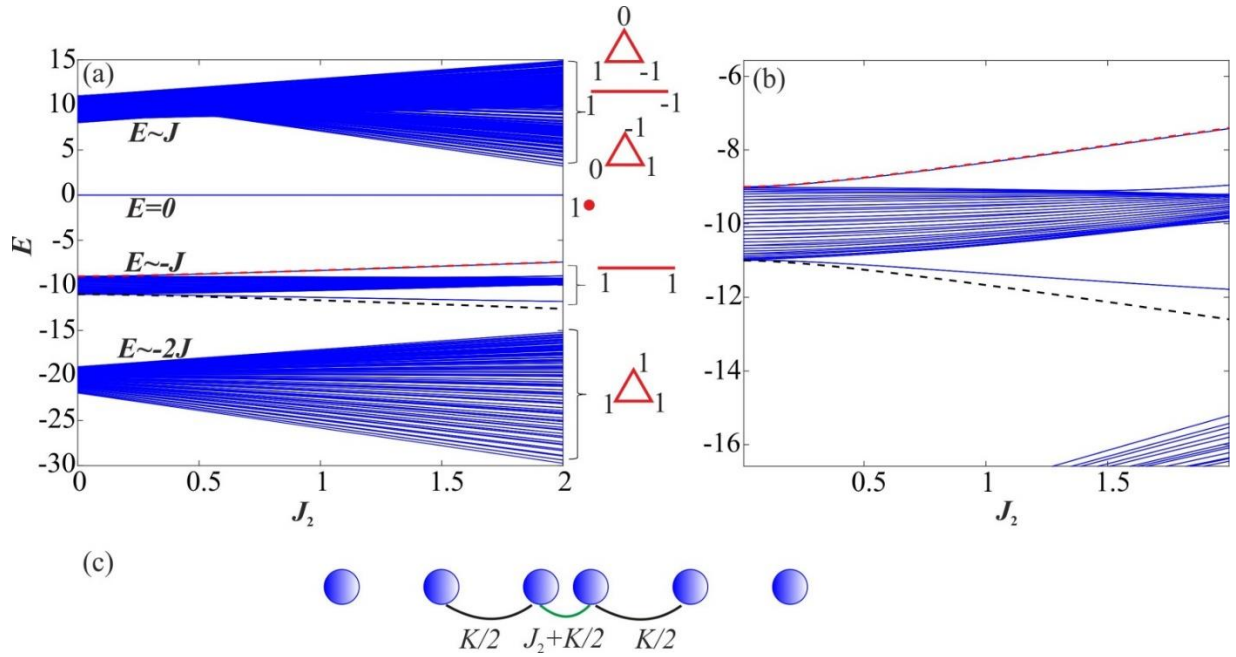

Fig. S7| (a) Eigenmodes of a finite lattice consisting of 630 sites calculated for $J/K = 10$ and for the ratio J_2/K varying in the range from 0 to 2. All modes split into four groups well-separated from each other. (b) Spectrum of the same system as in (a), showing the band of edge states and the emergence of a corner-localized state as the value of J_2 is increased. Red and black dashed lines show the analytical result for the energies of corner states obtained with first-order perturbation theory.

Bulk of the lattice consists of trimers [Fig. S6(b)] which support three types of multiply degenerate modes: one of them has equal amplitudes in all three sites of triangle and has the energy equal to $E = -2J$ [see the inset of Fig. S7(a)]; two other bulk modes with the amplitude distribution shown near the corresponding red triangles have energy equal to J. Once we assume some small but nonzero values of K or J_2, these modes give rise to the bulk bands depicted in Fig. S7.

In contrast, edge of the lattice consists of isolated dimers which support symmetric and antisymmetric modes with the energies scaling as $-J$ and J, respectively. Note that this set of modes gives rise to the edge states of the lattice.

Finally, corners of the lattice are represented by the isolated sites, and the energy of triply degenerate corner mode is equal to zero. Numerical calculation suggests that the energy of the corner mode remains zero even when both J_2 and K assume nonzero values as dictated by the symmetry of the lattice. This zero-energy corner mode appears even in the absence of next-nearest neighbor coupling, and we do not explore it any further.

Thus, in the limiting case $J_2 = K = 0$ we can easily calculate all modes of the lattice (which are simply the modes of the isolated trimers, dimers and monomers) and their respective energies. As a next step, we employ degenerate perturbation theory and deduce energy and the localization length of the corner mode facilitated by the next-nearest-neighbor coupling.

III. Degenerate perturbation theory in J_2 and K

Since we are looking only for the first-order corrections to the energies and wave functions of the lattice modes, it is sufficient to consider a single degenerate band neglecting its interactions with the rest of the bands. Indeed, the effects of band interaction result only in corrections quadratic

with respect to J_2 and K. Hence, we have to consider only the degenerate set of symmetric dimer modes with the energy equal to $-J$. For example, this set includes six edge modes in the situation of Fig. S5(a).

Including into the perturbation operator $\hat{V}$ all terms of the Hamiltonian proportional to K and J_2, we can immediately evaluate its matrix elements in the basis of symmetric modes of different dimers. For clarity, we write it for the geometry of Fig. S6, when it takes the form:

$$\hat{V} = -\begin{pmatrix} 0 & K/2 & 0 & 0 & 0 & 0 \\ K/2 & 0 & K/2 & 0 & 0 & 0 \\ 0 & K/2 & 0 & J_2 + K/2 & 0 & 0 \\ 0 & 0 & J_2 + K/2 & 0 & K/2 & 0 \\ 0 & 0 & 0 & K/2 & 0 & K/2 \\ 0 & 0 & 0 & 0 & K/2 & 0 \end{pmatrix} \tag{C4}$$

First-order corrections to the energies of the edge modes are then found as eigenvalues of the matrix Eq. (C4). To simplify our analysis further, we notice that this problem corresponds precisely to the tight-binding 1D lattice depicted in Fig. S7(c) and having modified coupling between the middle sites. Straightforward calculation yields the energies of defect-localized symmetric and antisymmetric modes

$$\delta E = \mp \frac{(K + 2J_2)^2 + K^2}{2K + 4\,J_2}, \tag{C5}$$

$$e^{i\kappa} = \pm \frac{K}{K + 2\,J_2}, \tag{C6}$$

where upper and lower signs correspond to symmetric and antisymmetric modes of the equivalent problem Fig. S7(c), respectively. In the original 2D problem, these modes translate to corner-localized modes with the field amplitude in the dimers decaying exponentially away from the corner as described by Eq. (C6) and with the energy given by

$$E = -J \mp \frac{(K + 2J_2)^2 + K^2}{2K + 4\,J_2}, \tag{C7}$$

whereas symmetric or antisymmetric nature of the corner modes is defined with respect to reflection relative to the bisectrix of the corner. For comparison, the energies of symmetric and antisymmetric corner modes calculated from Eq. (C7) are plotted by the black and red dashed lines in Fig. S7(b). It is seen that the lower energy symmetric mode strongly interacts with the continuum of the bulk states with energy $-2J$, and for larger K and J_2 quickly hybridizes with the continuum. At the same time, an antisymmetric corner mode appears to be more robust, featuring less pronounced interaction with the bulk bands and showing much better agreement with the first-order perturbation theory developed here. Note that it is this mode that was observed experimentally.

D. Numerical calculation of corner states in Kagome lattice considering all orders of long-range interaction as perturbation

To understand the role of all orders of long-range interactions, we use a simplified model where, in addition to the orders of coupling we have already considered (NN, NNN, 3rd NN), the longer range coupling coefficients drop with distance as $1/r$. The long-range couplings in real photonic system are dropping at least as *1/r* or faster (near-field components). We found that topological corner modes (both types) still exist when such weak long-range interactions are considered. Fig.

S8 shows the frequency distribution of corner and edge modes with all possible long-range interactions, proving that such perturbations do not destroy topological boundary modes.

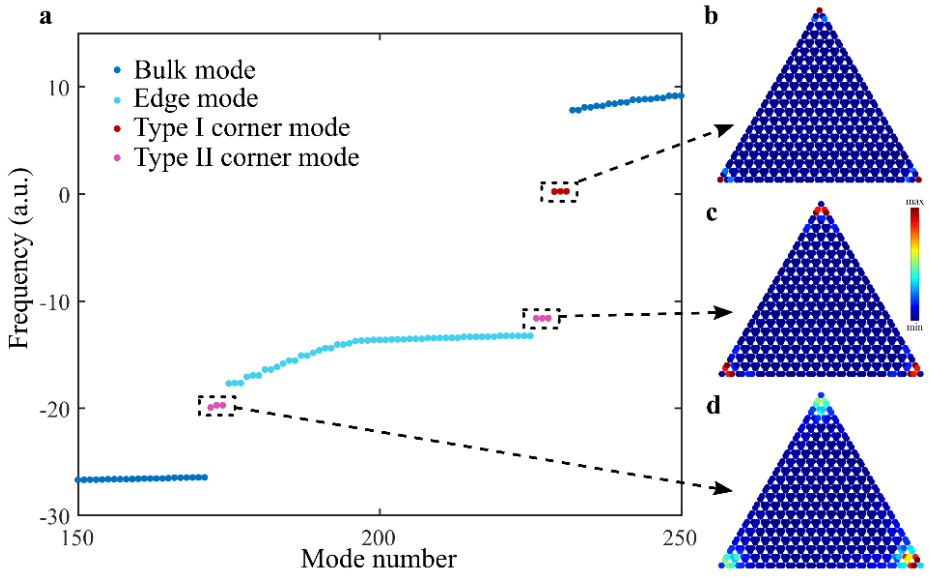

Fig. S8| Energy spectrum and corner state field profiles with all orders of long-range interactions in finite triangular shaped Kagome lattice. **a** energy (frequency) distribution of modes in long-range interaction system. **b**, **c** and **d** field profiles of corresponding corner states. $J/K = 3.5, J_2 = 0.75K, J_3 = 0.05K$ is used in the figures. Note that the triplet of "lower energy" type-II modes splits slightly into a singlet and a doublet of modes due to the finite size of the lattice and relatively slow decay of the field.

References

1. Ni X, Weiner M, Alu A, Khanikaev AB. Observation of higher-order topological acoustic states protected by generalized chiral symmetry. *Nat Mater* 2019, **18**(2)**:** 113.

2. Kingsmith RD, Vanderbilt D. Theory of Polarization of Crystalline Solids. *Phys Rev B* 1993, **47:** 1651.

3. Benalcazar WA, Bernevig BA, Hughes TL. Electric multipole moments, topological multipole moment pumping, and chiral hinge states in crystalline insulators. *Phys Rev B* 2017, **96:** 245115.

4. Pérez-González B, Bello M, Gómez-León Á, and Platero G. Interplay between long-range hopping and disorder in topological systems, *Phys Rev B* 2019, **99**: 035146.